NASA TECHNICAL NOTE

NASA TN D-5844

ANGULAR DISTRIBUTION
OF KAUFMAN ION THRUSTER BEAMS

by David C. Byers

Lewis Research Center
Cleveland, Ohio 44135

1. Report No. NASA TN D-5844	2. Government Accession No.	3. Recipient's Catalog No.
4. Title and Subtitle ANGULAR DISTRIBUTION OF KAUFMAN ION THRUSTER BEAMS		5. Report Date June 1970
		6. Performing Organization Code
7. Author(s) David C. Byers		8. Performing Organization Report No. E-5566
9. Performing Organization Name and Address Lewis Research Center National Aeronautics and Space Administration Cleveland, Ohio 44135		10. Work Unit No. 120-26
		11. Contract or Grant No.
		13. Type of Report and Period Covered
12. Sponsoring Agency Name and Address National Aeronautics and Space Administration Washington, D.C. 20546		Technical Note
		14. Sponsoring Agency Code

15. Supplementary Notes

16. Abstract

A collimating slit system was used to measure the ion beam envelope and thrust direction of a 15-cm-diam electron-bombardment thruster of the SERT II type. The angular distribution of the ion beam of five thruster configurations was investigated. The ion beam envelope was found to extend up to about 40° half-angle spread for the cases tested. The effect on thrust direction of a transverse grid misalinement was measured and found to compare well with previous experimental and theoretical results. The results of the study were applied to a proposed spacecraft design for a Jupiter flyby mission.

17. Key Words (Suggested by Author(s)) Electric propulsion Thrust vector Electron-bombardment ion	18. Distribution Statement Unclassified - unlimited		
19. Security Classif. (of this report) Unclassified	20. Security Classif. (of this page) Unclassified	21. No. of Pages 38	22. Price* $3.00

ANGULAR DISTRIBUTION OF KAUFMAN ION THRUSTER BEAMS

by David C. Byers

Lewis Research Center

SUMMARY

A collimating slit system was used to measure the ion beam envelope and thrust direction of a 15-centimeter-diameter electron-bombardment thruster of the SERT II type. The angular distribution of the ion beam of five thruster configurations was investigated. The ion beam envelope was found to extend up to about 40° half-angle spread for the cases tested. The effect on thrust direction of a transverse grid misalinement was measured and found to compare well with previous experimental and theoretical results. The results of the study were applied to a proposed spacecraft design for a Jupiter flyby mission. It was found that this design would suffer direct ion impingement on the solar cell panels for a major portion of the mission.

INTRODUCTION

Information concerning the thrust direction and ion beam envelope of electron bombardment ion thrusters is needed for both mission analysis and spacecraft design. The thrust vector of an individual thruster, or array of thrusters, must pass through the spacecraft center of mass to avoid disturbance torques. Uncertainties can exist in the thrust vector, however, because of initial component misalinements and possible time dependent variations due to thermal distortions (ref. 1). In particular, the thrust vector of a two grid electron-bombardment thruster is very sensitive to transverse misaline-ment of the accelerator grids (refs. 2, 3, and 4).

In addition to the need for initial specification of the thrust direction (ref. 5), control of the thrust vector during a mission is also of interest (ref. 6). Techniques to provide thrust vectoring capability include variation of grid alinement (ref. 4) with a two grid system, and variation of accelerator grid potential with a composite grid system (ref. 6). Therefore, determination of the relation between the thrust vector and its control variable is important.

Definition of the ion beam envelope is of considerable interest for spacecraft design

(refs. 7 and 8) in that it is important to avoid direct ion impingement on spacecraft components, such as solar cells and thermal control surfaces.

To date, the thrust vector of various electric propulsion devices has been evaluated by direct thrust measurements (refs. 9 and 10) and by the use of planar probes (ref. 4). The ion beam envelope has been evaluated with planar probes. Direct thrust measurement is, of course, the most straightforward means of defining the thrust vector. In practice, however, direct measurement of thrust direction is difficult due to the low thrust levels of the thrusters. Determination of the thrust vector with planar probes contains a potential error in that the direction of the ion current impinging on the probe cannot be specified. Ions may arrive at the planar probe with a variety of angles from various locations on the thruster. A thrust measurement, of course, does not specify the ion beam envelope. Failure to account for the finite source area of ions in the beam can contribute to possible errors in estimating the ion beam envelope with a planar probe. Curvilinear ion trajectories could also exist and would not be detected with a planar probe.

This report presents an experimental evaluation of the use of a collimating slit system (ref. 11) to determine thrust direction and to define the ion beam envelope of a two grid, mercury, electron-bombardment ion thruster. The effects of varying the grid alinement, accelerator grid voltage, grid-to-grid spacing, and ion beam current on the thrust direction and the ion beam envelope also were studied. Results are interpreted in terms of the affect on a specific spacecraft design (ref. 12).

APPARATUS

Figure 1 is a drawing of the experimental setup. A reference coordinate system is also shown. (All symbols are defined in appendix A.) A photograph of the experimental setup is shown in figure 2. The major components will be presented separately.

Thruster

The thruster used was of the SERT II type described in reference 13. The discharge chamber was 15 centimeters in diameter and a hollow cathode was used. Two vaporizers were used: one to provide a small amount of mercury propellant to the cathode, the other to provide the main portion of the mercury propellant directly to the discharge chamber. The accelerator grids were of flight-type SERT II design (ref. 5) and were identical to those described as set VI in reference 13. In the course of this investigation the grids were operated at grid-to-grid spacings of 2.54 and 3.81 millimeters. This
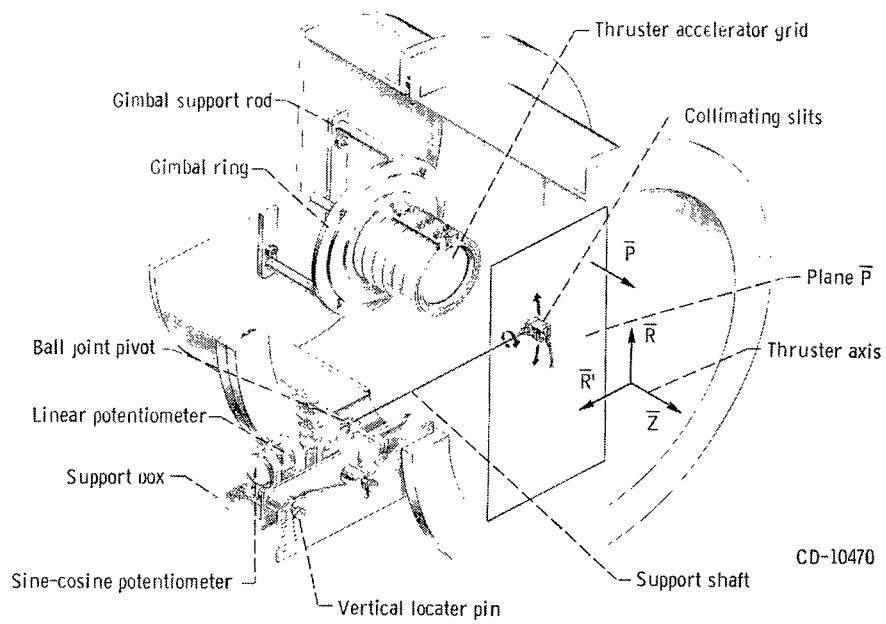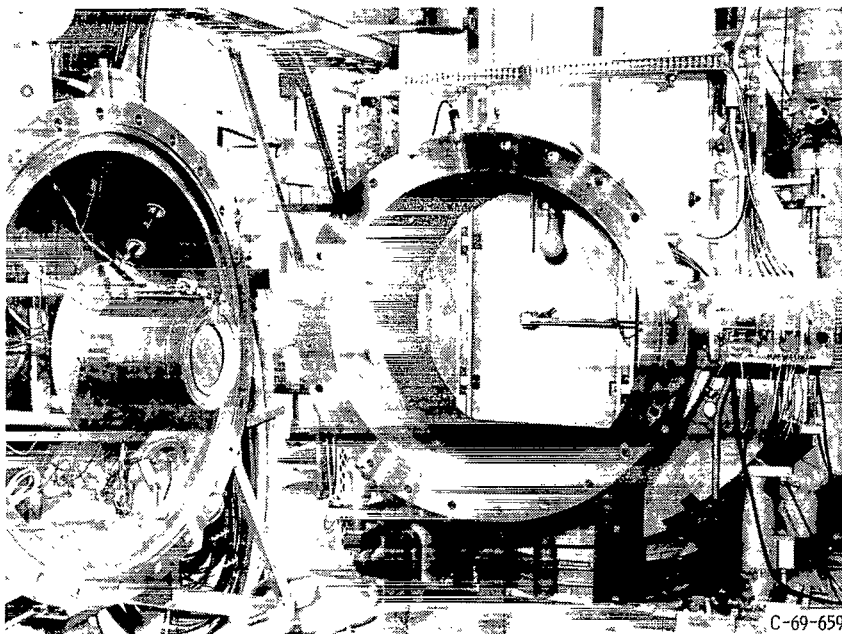
Figure 1. - Experimental setup.

Figure 2. - Thruster, slit system, and associated equipment.

spacing change was made by changing the diameters of the insulating standoff spheres between the grids. In one test the accelerator grid was shifted transversely 0.38 millimeter with respect to the screen grid. The transverse shift was made by cutting small extentions in the holes in which the standoff spheres were seated.

No neutralizer was used in this experiment. Beam neutralization was achieved by secondary electron emission from the vacuum tank walls. Neutralizer operation could possibly affect the ion beam characteristics but determination of such an effect was beyond the scope of this report.

The ion beam current magnitude was controlled via a feedback loop with the main propellant vaporizer. The indicated ion beam current was constant to within 0.4 percent for each of the thruster configurations tested. The discharge chamber voltage was set and the discharge chamber current was controlled by adjustment of the cathode propellant flow. To assure the stable operation during data taking periods, the thruster was operated for more than 2 hours prior to any data being taken. The discharge voltage and current were, after this stabilization period, constant to within 0.5 and 3 percent, respectively.

The thruster was mounted to a gimbal ring which in turn was mounted to the bell jar by means of four support rods (fig. 1). Thruster alinement was accomplished by adjustment of four screws holding the gimbal ring to the four support rods. For the data presented herein, the downstream face of the accelerator grid was perpendicular to the longitudinal axis of the bell jar to within 0.2^O. The center of the accelerator grid was within 0.4 millimeter of the longitudinal axis of the bell jar.
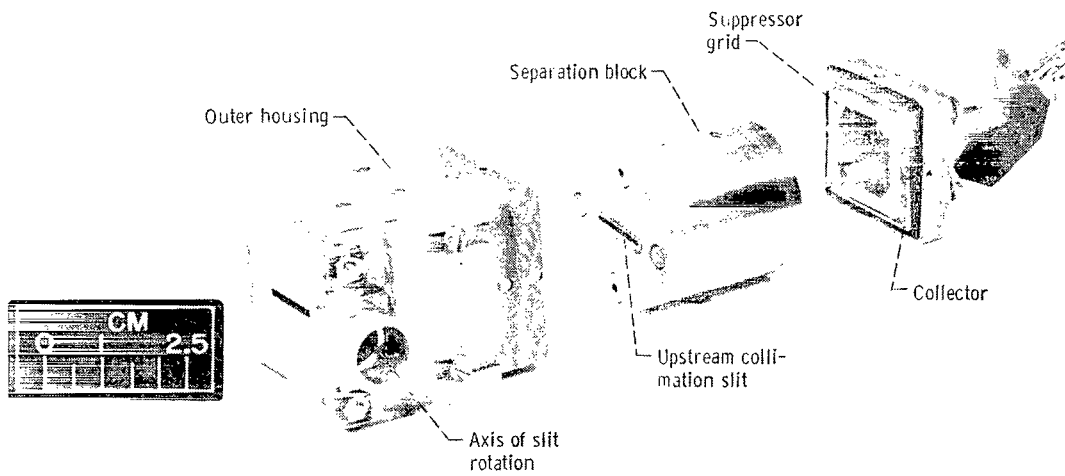
Collimating Slit System

An exploded view of the slit system, which was located 29.4 centimeters downstream of the thruster accelerator grid, is shown in figure 3(a), and a cutaway sketch of the slit system is shown in figure 3(b). The slit system consisted of:

(1) An outer housing and shield
(2) The two collimation slits and a separation block
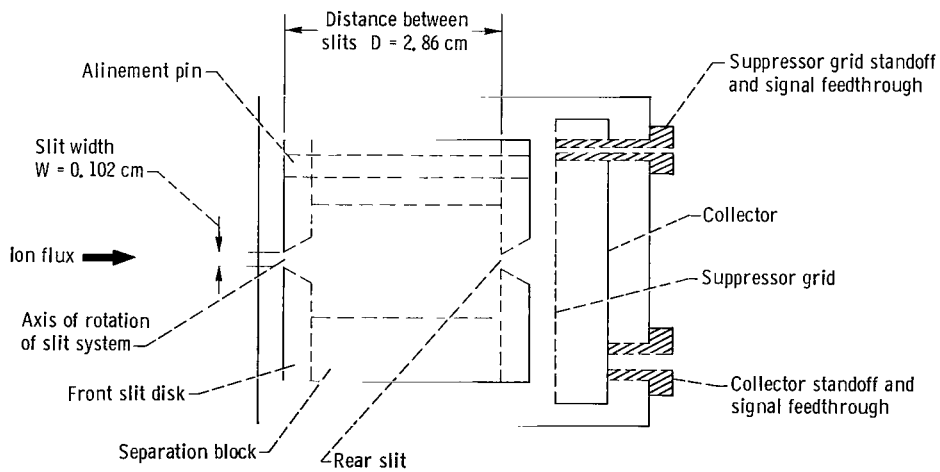(3) The collector and suppressor grid

The outer housing was made of aluminum and was covered with several layers of tantalum sheet. For clarity, the sheet is not shown in figure 3. The housing served to prevent the ion beam from impinging directly on the slits and separation block and also prevented extraneous electronic signals from reaching the collector.

The collimating slits were both 1.27 centimeters (0.5 in.) long by 1.02 millimeters (0.040 in.) wide and were milled from 3.18-millimeter-thick nonmagnetic stainless steel disks. The dimensions of the slit and separation block were accurate to 0.05 mil-

4

Outer housing

Separation block

Suppressor grid

Collector

Upstream colli-
mation slit

Axis of slit
rotation

(a) Exploded view.

C-69-901

Distance between
slits D = 2.86 cm

Alinement pin

Slit width
W = 0.102 cm

Ion flux

Axis of rotation
of slit system

Front slit disk

Separation block

Rear slit

Suppressor grid standoff
and signal feedthrough

Collector

Suppressor grid

Collector standoff and
signal feedthrough

(b) Cutaway view.

Figure 3. - Collimating slit system.

5

limeter. The edges of both slits were beveled at an angle of about 60° to provide sharp slit edge definition. The beveled sides were on the downstream side of both slits (fig. 3(b)). The width of the slits was selected arbitrarily. As will be shown later, the signal-noise ratio was such that slits of less than half the width of those used herein could have been used.

The slit disks were attached directly to the 2.54-centimeter-long separation block by screws. The separation block was a 3.18-centimeter outside diameter, 1.9-centimeter inside diameter cylinder made of nonmagnetic stainless steel. The distance between the slits was about 2.86 centimeters. Close alinement of the slits was accomplished with alinement rods that were inserted through holes in the disk-separator system. After assembly, the slit-separator unit was mounted directly to the outer housing by screws.

The collector was made of 0.38-millimeter-thick tantalum and the suppressor grid consisted of 0.13-millimeter-diameter tantalum wires strung on a 2-millimeter-square grid. The open area fraction of the suppressor grid was about 0.88. The collector and the suppressor grid could be biased together either positively or negatively with respect to ground (fig. 4). In addition, the suppressor grid could be biased positively or negatively with respect to the collector.

Support Shaft and Associated Equipment

One purpose of this experiment was to determine the directional properties of the ion beam along a diameter of the thruster. Therefore, the collimating slit system was made so that it could be moved across the beam in a near vertical direction in plane $\overline{P}$
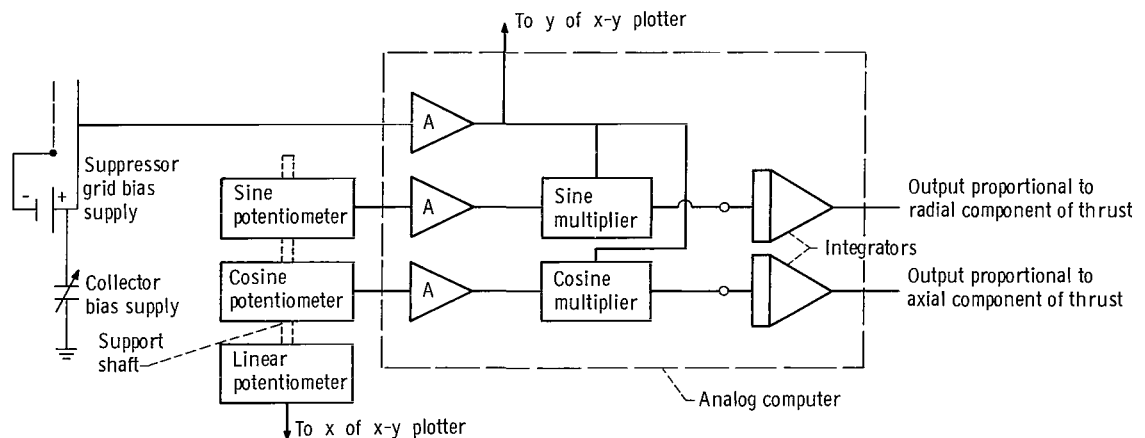

Figure 4. - Simplified electrical schematic of collimating slit system electronics.

(along a line which was approximately parallel to a thruster diameter) and rotated at each position (see fig. 1). Plane $\overline{P}$ was perpendicular to the thruster axis and parallel to the plane of the accelerator grid. The angle between the longitudinal axes of the thruster and the slit system varied as the slit system was rotated. This angle will hereinafter be called the dispersion angle, following reference 14. The basic data of the experiment was then the variation of ion current with dispersion angle at various probe positions in plane $\overline{P}$.

The rotation of the slit system to various dispersion angles was achieved by rotation of the support shaft (see fig. 1), the axis of which was centered on the short dimension and parallel with the long dimension of the slit that was located closest to the thruster. Thus, the axis of the support shaft and the long centerline of the closest slit were at all times located in plane $\overline{P}$ (fig. 1). The support shaft and some associated equipment were mounted on an aluminum box. A constant speed electric motor was used to rotate the shaft, hence the slit system, at each slit system position. The constant rate of shaft rotation was necessary since the collector signals were to be integrated. Several checks indicated that the time to rotate through 180° was constant to better than 0.2 percent.

The vertical position of the slit system was varied by pivoting the support shaft about a pivot located in a ball joint vacuum seal on the bell jar wall (fig. 1). A locater pin was mounted to the aluminum support box. Vertical probe positions were fixed by press fitting the locater pin into holes drilled into a 0.63-centimeter-thick aluminum plate which was mounted to the tank. The aluminum box, which contained the support shaft, could also be clamped to the aluminum plate to fix its position. The positioning accuracy of the system was about 0.4 millimeter.

With the technique used to change the vertical location, the slit system actually traversed a slight arc in plane $\overline{P}$ (see fig. 1) rather than a true vertical line along a diameter of the thruster. As a result, the long axis of the slit system was not exactly perpendicular to a thruster diameter when the front slit was not on the thruster axis. The angle between the long slit axis and a thruster diameter varied from about 90° to 80° as the vertical position was varied from 0 (on the thruster axis) to 21.1 centimeters (the largest vertical distance at which data were taken). The exact effect of the deviation from perpendicularity of the slit axis and a thruster diameter is not known, but is believed to be small and was neglected in this report. A linear positioning mechanism (which would be more complex than the vertical positioning technique used herein) would allow vertical measurements to be taken exactly along a thruster diameter.

Electrical Circuitry

A simplified electrical schematic is shown in figure 4. Both a linear and a sine-

cosine potentiometer were attached to the support shaft. The output of the linear potentiometer was directly proportional to the dispersion angle of the slit system. The sine output of the sine-cosine potentiometer was adjusted to yield 0 and ±10 volts at dispersion angles of 0° and ±90°, respectively. The cosine output was adjusted to yield 10 and 0 volts at dispersion angles of 0° and ±90°, respectively. It was found that the absolute value of the output of the sine potentiometer was low by about 4 percent. This correction was included in all data presented herein. The output of the cosine potentiometer was accurate to within 0.5 percent and no correction was made.

An analog computer was used to condition the signals from the collector and the sine-cosine potentiometer. The main elements of the analog computer are shown within the dashed line of figure 4. The three input signals were first fed into unitary gain amplifiers (marked A on fig. 4). The collimated current signal and the signals proportional to the sine and the cosine were fed into separate multipliers. The outputs of these multipliers were then fed to two separate integrators, whose outputs were used to determine the ratios of the radial and axial components of thrust at the particular radial position. The analog computer system was calibrated with the use of a separate power supply. The output of the calibration power supply was monitored by a microammeter and fed to ground through a precision resistor. The voltage signal from the precision resistor was fed to the collector current input of the analog computer. Calibration of the outputs of the integrators was then achieved directly in terms of a known input signal.

Vacuum Facility

The vacuum tank in which the tests were conducted was 1.5 meters in diameter by 4.5 meters in length. The thruster was mounted in the metal bell jar (fig. 1) separated from the main tank by a 0.9-meter-diameter gate valve. The tank was pumped with four 0.8-meter-diameter oil diffusion pumps with liquid-nitrogen-cooled baffles. The pressure measured in the bell jar was less than 5×10^{-6} torr for all the data presented herein.

TEST PROCEDURE

With the thruster in operation, the collimating slit system was positioned in the ion beam and the support shaft was rotated through 180°. A voltage proportional to the collimated current which passed through the slit system was fed simultaneously to the analog computer and the y axis of an x-y plotter. A signal proportional to the angle of rotation was fed to the x axis of the x-y plotter from the linear potentiometer attached to the support shaft. Signals proportional to the sine and cosine of the angle of rotation (from

the sine-cosine potentiometer) were also fed to the computer. The collimated current signal was multiplied simultaneously by the signals proportional to the sine and cosine of the angle of rotation. These multiplied signals were then integrated and read out on two digital voltmeters. Details of analysis of the x-y plotter traces and the other data outputs are presented in appendix B. A discussion of experimental errors is included as appendix C.

At each radial location the following types of output data were obtained:

(1) An x-y plotter trace of the collimated current as a function of the angle of rotation. This output provided convenient and permanent graphical presentation of the ion current density as a function of dispersion angle.

(2) The integrals of the product of the collimated current with both the sine and cosine of the angle of rotation. The first integral was used to determine the radial component of thrust at each location. The latter integral was used to determine the axial component of thrust and was proportional to the ion current passing through plane $\overline{P}$.

Values proportional to the radial and axial components of thrust obtained at each location were plotted as a function of the radial distance from the axis of the thruster and a smooth curve was drawn through these data. Hand integration of these curves provided numbers proportional to the total axial and radial components of thrust in the survey plane. The total thruster ion beam current was calculated by integration of the curve of current density obtained at each location plotted as a function of radial distance from the axis of the thruster.

RESULTS AND DISCUSSION

In this section, the ion beam current density distribution and the thrust direction results of the standard thruster (case I) are presented first. The ion beam characteristics of the standard configuration with the accelerator grid shifted transversely by 0.38 millimeter (case II) are then discussed and compared with previous theoretical and experimental results (refs. 2, 3, and 4). Some effects on the beam envelope and thrust direction are then presented for variations of accelerator grid voltage (case III), grid-to-grid spacing (case IV), and ion beam current (case V). Finally, some implications of the experimental results on a proposed spacecraft design (ref. 12) are discussed.

Standard Thruster (Case I)

The standard thruster was nearly identical to the SERT II thruster described in ref-

TABLE I. - THRUSTER OPERATING PARAMETERS

[Net accelerating voltage V_I = 2000 V.]

Case	Description	Accelerator grid voltage, V_A, V	Ion beam current, J_B, A	Discharge chamber voltage, ΔV_I, V	Discharge chamber current, J_I, A	Grid-to-grid spacing, l, mm
I	Standard thruster	2900	0.242	37.0	2.00	2.54±0.13
II	Misalined grids	2900	.242	37.2	1.95	2.54±0.13
III	Low accelerator grid voltage	1000	.242	37.0	2.22	2.54±0.13
IV	Increased grid spacing	2900	.241	36.9	2.05	3.80±0.13
V	Low beam current	2900	.155	41.7	.95	2.54±0.13

erences 5 and 13. Significant operating parameters are presented in table I. The thruster operating conditions were those of the nominal operating point of the SERT II flight thruster with three exceptions. First, no neutralizer was used. Second, the screen and accelerator grid voltages were 2000 and -2900 volts, respectively. The net accelerating voltage was lowered from the SERT II value of 3000 volts to decrease the energy level of ions incident on the slit system. The accelerator grid voltage was increased to -2900 volts (the maximum output of the supply) so that the total accelerating voltage of 4900 volts would be similar (within 100 V) to that of the SERT II thruster. Finally, the total ion beam current was 0.242 ampere instead of the 0.250 ampere of the SERT II thruster at design operating point.

Several geometric variables relating the slit positioning to the thruster axis and thruster configuration are shown and defined in sketch (a). (Drawing not to scale.)

(a)
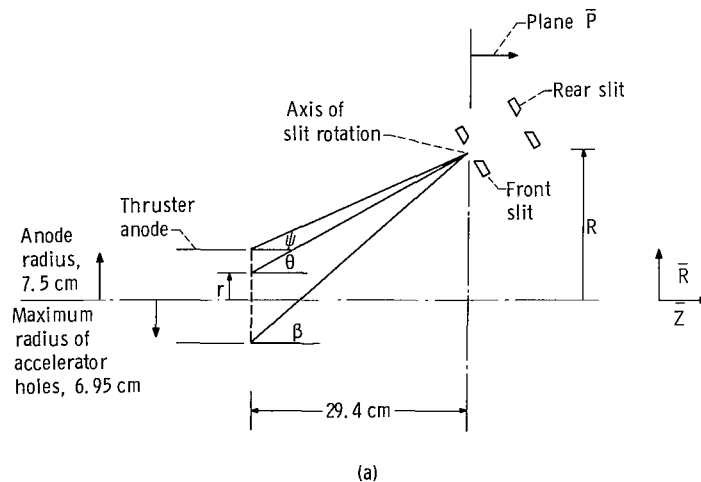
The dispersion angle θ is the angle between the longitudinal axis of the slit system and a line drawn parallel to the thruster axis. The vertical slit system position R was measured in the $\overline{P}$ plane from the point of intersection of the thruster axis and the $\overline{P}$ plane. As mentioned previously, the $\overline{P}$ plane was parallel to and 29.4 centimeters downstream of the accelerator grid. The distance, measured in the plane of the accelerator grid, between the thruster axis and the projected slit system axis is shown as r in sketch (a). Effectively, the value of r indicated where the slit system was pointed on the accelerator grid. While the thruster anode was 7.5 centimeters in radius, the holes of the accelerator grid (the source of the ions) were contained within a radius of 6.95 centimeters. The values of θ, r, and R were all taken to be positive upward.

Figure 5 shows the x-y plotter traces of the ion current density as a function of the dispersion angle θ and the variable r at four slit system positions. When the slit system was on the axis of the thruster (fig. 5(a)), the collected current was nearly symmetric about a dispersion angle of 0°. This symmetry implied a negligible net radial component of thrust of the ion beam at this position. It is also seen the collected current became negligible at dispersion angles greater than about $\pm16^O$. These values of dispersion angle correspond to values of r of about ∓7.0 centimeters, respectively.
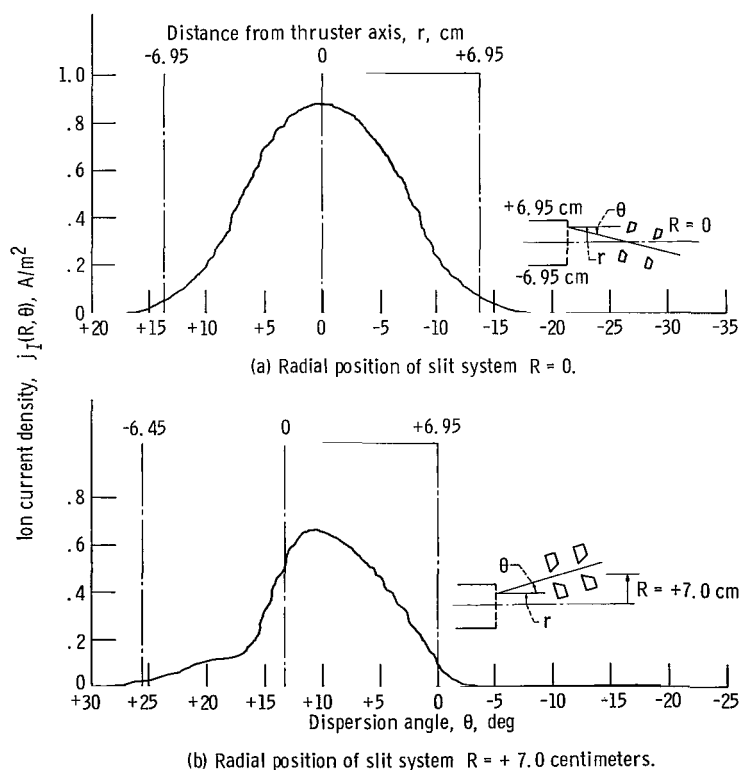

(a) Radial position of slit system R = 0.

(b) Radial position of slit system R = + 7.0 centimeters.

Figure 5. – Ion current density as function of dispersion angle; standard thruster (case I). (Insert not to scale.)

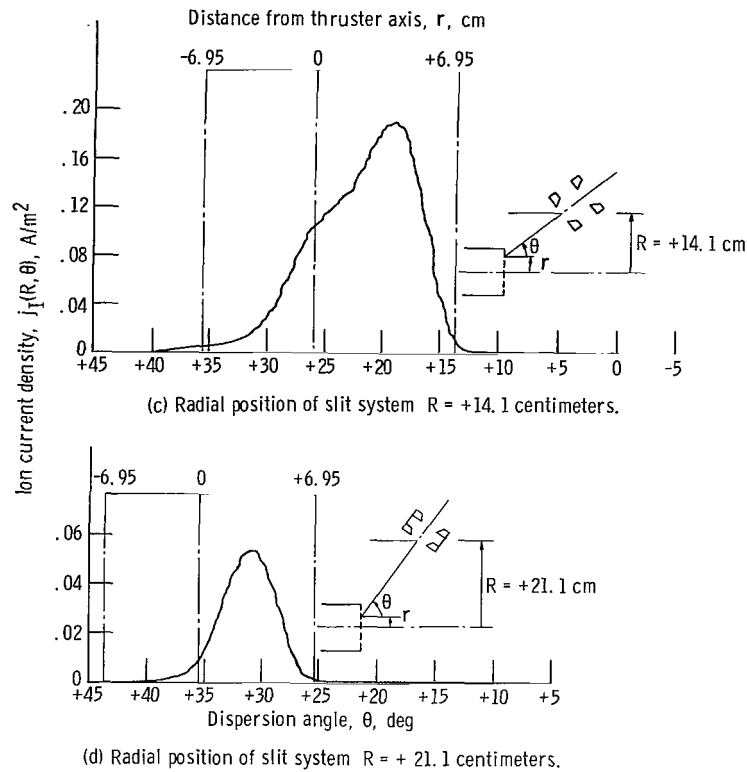Distance from thruster axis, r, cm

-6.95　　　0　　　+6.95

.20

.16

.12

.08

.04

0

Ion current density, $j_I(R, \theta)$, A/m²

R = +14.1 cm

+45　+40　+35　+30　+25　+20　+15　+10　+5　0　-5

(c) Radial position of slit system R = +14.1 centimeters.

-6.95　　0　　+6.95

.06

.04

.02

0

R = +21.1 cm

+45　+40　+35　+30　+25　+20　+15　+10　+5

Dispersion angle, θ, deg

(d) Radial position of slit system R = +21.1 centimeters.

Figure 5. – Concluded.

Essentially then, little current was collected when the slit system was pointed at a point beyond the radius within which all the accelerator holes were contained. This was true for all thruster configurations tested at all radial positions at which data were taken.

Figure 5(b) shows that plotter trace at a probe radial position of +7.0 centimeters. It is seen that the current peaked at a dispersion angle of about 11° and a corresponding value of r of about 1.5 centimeters. The absolute values of dispersion angle at the maximum of collected current increased with vertical slit position R for all thruster configurations tested. A plotter trace taken at the opposite vertical position (-7.0 cm) was quite similar to figure 5(b). This similarity existed at all the vertical positions at which data were taken with the standard (case I) thruster configuration. This fact implied that negligible net radial thrust was produced with the standard thruster configuration. As will be shown in a subsequent section, this absence of significant radial thrust was verified with the analog computer outputs.

Figures 5(c) and (d) show the plotter traces with the slit system at vertical distances of 14.1 and 21.1 centimeters, the largest vertical distance at which data were taken. It is seen that the dispersion angle at the peak current was about 19° and 31° at vertical slit positions of 14.1 and 21.1 centimeters, respectively.

Figure 5(d) can be used to indicate the error that can exist in the use of planar probes to define the beam envelope. The half-angle for beam spread is usually defined (ref. 9) as the angle between a line parallel to the axis of the thruster located at the anode radius and a line drawn to the probe from the downstream side of the accelerator grid (shown as angle ψ in sketch (a)). At the maximum vertical slit position of 21.1 centimeters, the usually defined half-angle would be about 24.8°. It is seen, however, from figure 5(d) that the dispersion angle at the maximum value of collected current was about 6° greater than the geometrically defined half-angle. In addition, ion current was collected at dispersion angles up to about 15° greater than the geometric half-angle. The dispersion angles of the ions in the beam can, therefore, be considerably higher than those estimated in the usual fashion from a planar probe trace of the ion beam. As mentioned previously, negligible current was collected when the absolute value of r was greater than 6.95 centimeters. Therefore, a planar probe trace could be used to estimate maximum half-angles more meaningfully if the reference point on the thruster was taken at the anode radius on the side of the thruster opposite that of the planar probe. A half-angle of ion beam spread defined in this fashion is shown as angle β in sketch (a).

The x-y plotter traces can be used in a slightly different application to determine the fraction of the total beam current contained within various dispersion angles. To accomplish this, each x-y plotter trace was divided into increments of 5°. The area under the curve between 5° increments was divided by the total area under the curve. This ratio represented the fraction of the total ion current in that 5° increment at that particular vertical slit location. The fraction was taken to be constant over a distance equal to the vertical distance between slit data point locations. In order to relate the local values to the total, ion beam axial symmetry was assumed and the fractions were weighted by the R-distance at which the particular data were taken. The results of this analysis are shown in figure 6 which presents the fraction of the ion beam contained within the dispersion angle shown on the abscissa. It is seen that 80 percent of the ion beam was within a dispersion angle of 20°.

Possible sources of the measured ion current, especially the ion current at large dispersion angles, are either primary ions from the thruster or charge-exchange ions produced between the accelerator grids or downstream of the thruster.

Reference 14 presented a theoretical estimate of the number of and dispersion angles of charge-exchange ions produced by a 15-centimeter-diameter thruster. The thruster model conditions in reference 14 were an ion beam current of 0.239 ampere, a propellant utilization efficiency of 0.8, and screen and accelerator grid voltages of 3000 and -2000 volts, respectively, compared with 2000 and -2900 volts used herein. Reference 14 indicated that the charge-exchange ion current produced between the accelerator grids was about 0.4 percent of the total ion beam current. The total number of charge-exchange ions, produced between the grids, which would escape the thruster at
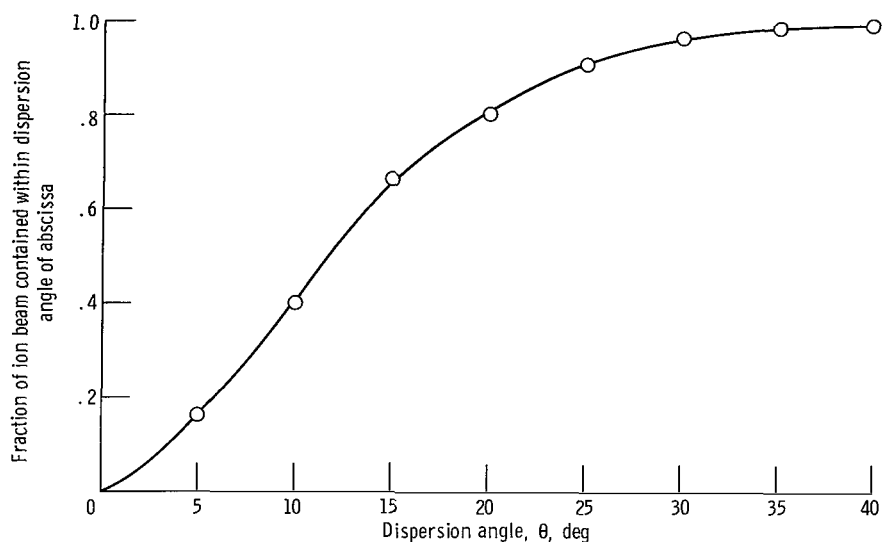
Figure 6. - Fraction of ion beam contained within various dispersion angles. Standard thruster (case I).

dispersion angles greater than 20°, however, was only about 0.02 percent of the ion beam. Reference 14 also calculated the number of charge-exchange ions produced downstream of the accelerator grid. These ions could have large dispersion angles due to the absence of strong focusing electric fields. In the calculation, the neutral background gas density was assumed to be due to neutral efflux from the thruster as calculated in reference 15. The total number of charge-exchange ions produced in a cylinder which extended 22 centimeters downstream of the accelerator grid was calculated to be less than 2 percent of the ion beam. Therefore, the total number of charge-exchange ions produced with dispersion angles greater than 20°, as calculated based on reference 14, was much less than the fraction with dispersion angles greater than 20° observed in this experiment (about 2 percent compared with 20 percent). In addition, because of a higher propellant utilization efficiency in the present experiment, the number of charge-exchange ions formed by the thruster would be expected to be less than that predicted in reference 14.

These remarks indicate that the observed ion current in this experiment is essentially composed of primary ions from the thruster. The fraction of ions at dispersion angles greater than 20° is clearly higher than that predicted from theoretical studies of grid configurations similar to the SERT II conditions (refs. 2, 3, and 16). However, this result may arise because of the differences in applied grid voltages. Variations in applied grid voltages are known to affect trajectories of ions leaving the thruster. As shown later, tests with the collimation slit system indicate accelerator grid voltage can strongly affect the local ion current densities and the local angular distribution of ion current density with dispersion angle.

14

The results of figure 6 can be used to estimate the net thrust of the standard thruster configuration. The plot was divided into increments of 5°. The fraction of the total ion current within a 5° increment was assumed to have a dispersion angle equal to the average dispersion angle for that particular increment. The fraction of current in each increment was then weighted by the cosine of the average dispersion angle. The results of this procedure indicated that for the standard (case I) configuration the thrust was about 5 percent less than that calculated directly from the net accelerating potential and ion beam current. Figure 7 shows the ion current density profile of the standard grid as de-
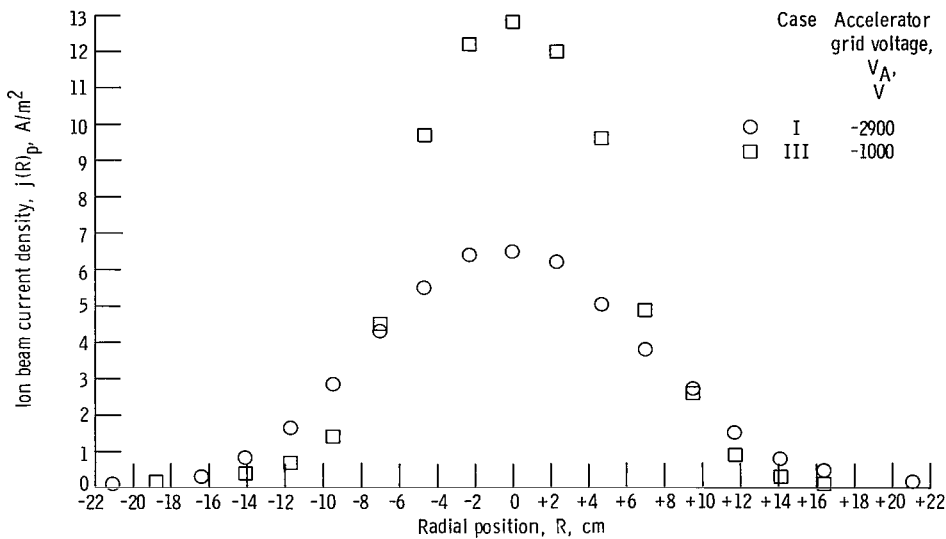

Figure 7. - Ion beam current density profile 29.4 centimeters downstream of accelerator grid.

termined from the analog computer output. The technique for obtaining the data is detailed in appendix B. For later reference, a profile is also shown for the standard thruster with the accelerator grid voltage reduced by 1900 volts (case III).

As a check on overall system accuracy, the profiles of figure 7 were hand integrated to obtain the total ion beam current. Details of the integration procedure also are discussed in appendix B. The total currents obtained by integration of the traces of figure 7 were 0.219 and 0.222 ampere for cases I and III, respectively. These calculated values are about 9 percent lower than the beam currents measured with an ammeter for both cases (table I). A discussion of possible reasons for the discrepancy between the total ion beam current determined by the two techniques is presented in appendix C.

The direction of the thrust vector was determined by use of the outputs of the analog computer (appendix B). Figures 8(a) and (b) show the outputs proportional to the radial and axial component of thrust, respectively, for the standard configuration. For later
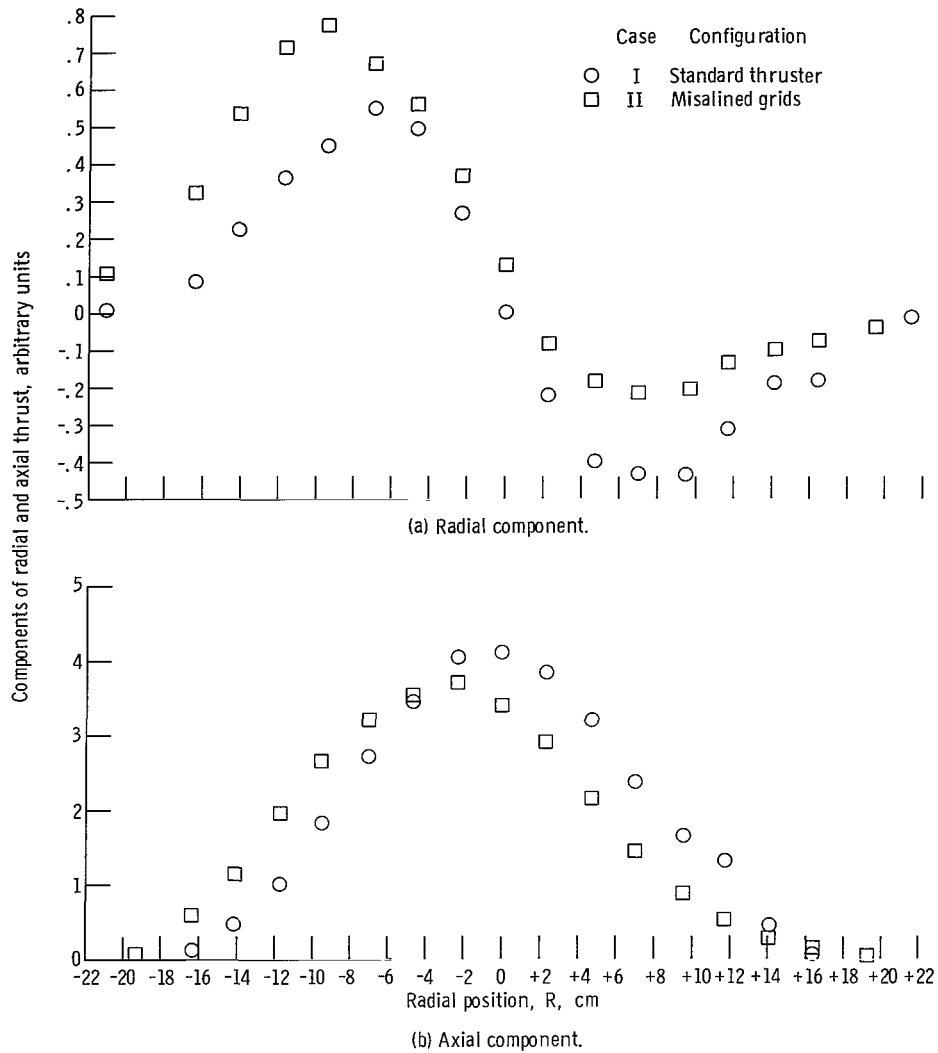
15

Figure 8. – Components of thrust as function of radial distance.

reference, similar data are shown for the standard thruster with misalined grids (case II).

The total radial and axial thrust in the survey plane $\bar{P}$ is proportional to the net area under the curves of figures 8(a) and (b), respectively. Based on these areas, the direction the thrust vector in the survey plane was found to be parallel to the thruster axis to within 0.2° for case I.

Misalined Grids (Case II)

The effect on ion beam envelope and thrust direction due to a transverse misaline-

ment of the accelerator grid of 0.38 millimeter was investigated and the result is compared in figure 9 with the results of other investigators. The accelerator grid was displaced in a positive vertical direction and, in agreement with references 2, 3, and 4, the ion beam was deflected in a negative direction. It is seen from figure 9 that the measured thrust deflection was in fairly good agreement with results of references 2 and 4 and was somewhat less than that predicted by reference 3. The deflection obtained in reference 3, however, referred to the maximum ion deflection and not the thrust vector. The deflection obtained in reference 2 referred to thrust deflection which is somewhat less than the maximum ion trajectory deflection.

Figure 10 shows the local ion current density distribution for the misalined grid (case II) as a function of dispersion angle at values of R of ±21.1 centimeters. The maximum ion current density in the direction of the beam deflection (fig. 10(a)) was about four times greater than that in the opposite direction (fig. 10(b)). The spread in the dispersion angle in the direction of deflection was about twice that in the opposite direction.

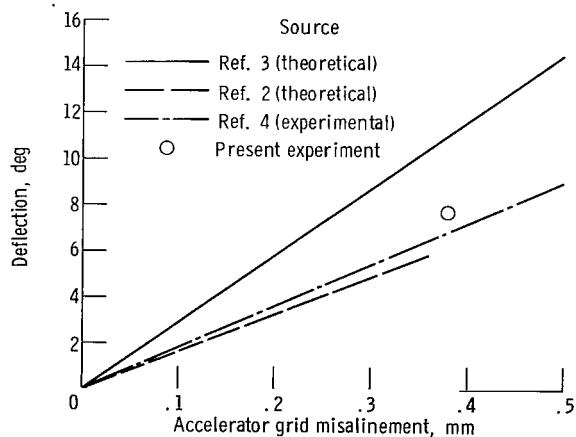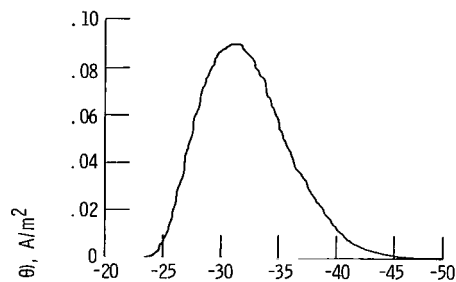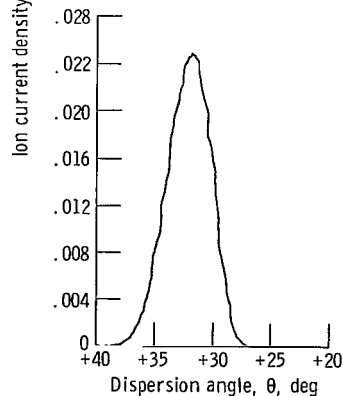Table II presents the average ion beam current density at various vertical slit posi-

Figure 9. - Beam deflection as function of accelerator grid transverse misalinement.

(a) Radial position R = -21.1 centimeters.

(b) Radial position R = +21.1 centimeters.

Figure 10. - Ion current density as function of dispersion angle. Misalined grids (case II).

TABLE II. - SOME ION BEAM CHARACTERISTICS

Case	Description	Radial position of slit system, R, cm	Average ion current density, $j(R)_p$, A/m^2	Dispersion angle at maximum of collected current, θ, deg	Range of dispersion angles over which ion current was collected, θ, deg
I	Standard thruster	+21.1	0.16	+31	+26 to +39
II	Misalined grids	+21.1	.062	+32	+27 to +38
		-21.1	.41	+31	-24 to -45
III	Low accelerator grid voltage	+21.1	.006	+25	+22 to +27
IV	Increased grid spacing	-21.1	.06	-29	-26 to -33
V	Low beam current	+21.1	No data	+33	+27 to +39

tions. The technique used to obtain these values is given in appendix B. Also shown in table II is the dispersion angle at which the ion current density was a maximum and the range of dispersion angles within which ion current was collected at the particular slit system radial position. The ion beam characteristics are presented at the largest radial distance at which data were taken (21.1 cm) because these data relate directly to the ion beam envelope definition.

Data presented in table II show that the grid misalinement caused an increase (relative to the standard configuration) in ion current density of about 2.6 in the direction of thrust deflection. Conversely, the value of current density in the direction away from thrust deflection was decreased by nearly the same factor. The maximum absolute value of dispersion angle at which current was collected increased to 45° in the direction of thrust deflection but remained nearly the same in the opposite direction. The data shows the importance to the spacecraft designer of knowing the total effects of all parameters on the ion beam envelope.

Accelerator Grid Voltage (Case III)

The accelerator grid voltage was lowered to -1000 volts to determine the effect on ion beam characteristics. The operating conditions for this test are shown in table I. Figure 7 showed the ion beam profile for case III. It is seen that the effect of lowering the accelerator voltage was to nearly double the ion current density (measured at plane $\overline{P}$) in the center of the beam. The case III ion current density and dispersion angle char-

acteristics at a radial distance of 21.1 centimeters are also presented in table II. It is seen that the currents were much reduced at this radius from those of the standard thruster configuration. Also the maximum value of the dispersion angle at which current was collected was reduced by about 12° from that of the standard configuration.

The observed effect with accelerator grid voltage was somewhat surprising, since, as the accelerator grid voltage was reduced it is likely that the discharge chamber plasma sheath at the screen grid became less concave toward the accelerator grid. Such a plasma sheath change might be expected to increase the ion dispersion angles and beam spread. However, significant ion crossover may have existed with the standard thruster configuration. Also, operation at reduced accelerator voltage may have caused a reduction of ion trajectory curvature in the acceleration region. It is also possible that the radial distribution of ions within the discharge chamber is affected by the accelerator voltage.

Grid-to-Grid Spacing (Case IV)

A test was performed with a grid-to-grid spacing of 3.8 millimeters. A marked increase in the impingement current on the accelerator grid occurred for ion beam currents in excess of 0.254 ampere. This behavior was most probably due to defocusing of the beam in the acceleration region. To avoid warpage of the grid, the ion beam current was lowered to 0.242 ampere. The data of table II show that the ion current density was reduced from that of the standard configuration by about a factor of three at a radial distance of 21.1 centimeters. In addition, the maximum dispersion angle at which ion current was detected was reduced by about 6° from the standard case.

Ion Beam Current (Case V)

The ion beam current was reduced to 0.155 ampere to determine the effect of ion beam current on the ion beam envelope. Values of x-y plotter scale factors were unavailable for this test so that ion current density calculations were not made. It is seen in table II that, although the ion beam current was reduced, the dispersion angles within which current was collected was nearly the same as for case I. The maximum measured density occurred, in fact, at a dispersion angle 2^O greater than for case I.

Effects on a Proposed Spacecraft Design

The results of these experiments indicated that the beam envelope could be sensitive to some operating conditions of the thruster. In addition, the beam envelope changed with grid alinement. With an interplanetary solar powered electric propulsion spacecraft, the operating parameters of the ion thruster can be expected to change during a mission. This arises from both the fact that the available power to the solar array varies with distance from the Sun and that the solar cell efficiency varies with time (ref. 17). As a result, it is of interest to apply the results obtained in this report to a particular spacecraft design. The spacecraft design chosen was that proposed in reference 12 for a Jupiter flyby mission.

A view of the spacecraft is shown in figure 11 (fig. 1-4 of ref. 12). Five thrusters and the solar cell panels are shown. During the mission, the thrusters would rotate through about 105° relative to the solar panels. At about 80 days into the proposed mission, the longitudinal axes of the thrusters will be parallel to the plane of the solar cells. The design of the solar cell array was such as to provide an escape cone of about 30° half-angle for the thruster exhaust.

In order to relate the results reported herein with this particular spacecraft design, it is necessary to discuss ion impingement at a particular reference point on the solar cells. The points marked A on the solar cell panels (fig. 11) are the reference points that will be used for this discussion. When the thrusters are parallel to the plane of the solar cells, point A is about 8.5 meters axially downstream of the thruster exhaust plane and about 6.1 meters radially from the axis of the central thruster. The dispersion angles of the ions in the central thruster primary ion exhaust must be less than about 35.5^O to avoid impinging on point A on the solar panels. In addition, the dispersion angles of the ion beams of the outboard thrusters must be less than about 30° to avoid impingement on the solar cells.

Table II shows that, for several thruster configurations, and the orientation described, ions would impinge on the solar cells at the 80-day point of the mission. Specifically, for the standard thruster about 1 percent of the total ion beam from the center thruster would be at a dispersion angle sufficient for some of these ions to impinge on the solar cells. Of course, due to a symmetrical distribution of ions in the beam only a small fraction of these would actually impinge on the panels. The ion impingement would persist until the longitudinal axis of the thrusters rotated out of the plane of the solar cells. A calculation indicated that the ion flux from the central thruster (at a dispersion angle of 39°) would impinge on the solar cells (point A) for about 130 days of the mission. The ion flux from the outboard thrusters would impinge on the solar cells for a somewhat longer period.

The previous discussion is included only to emphasize the importance of definition
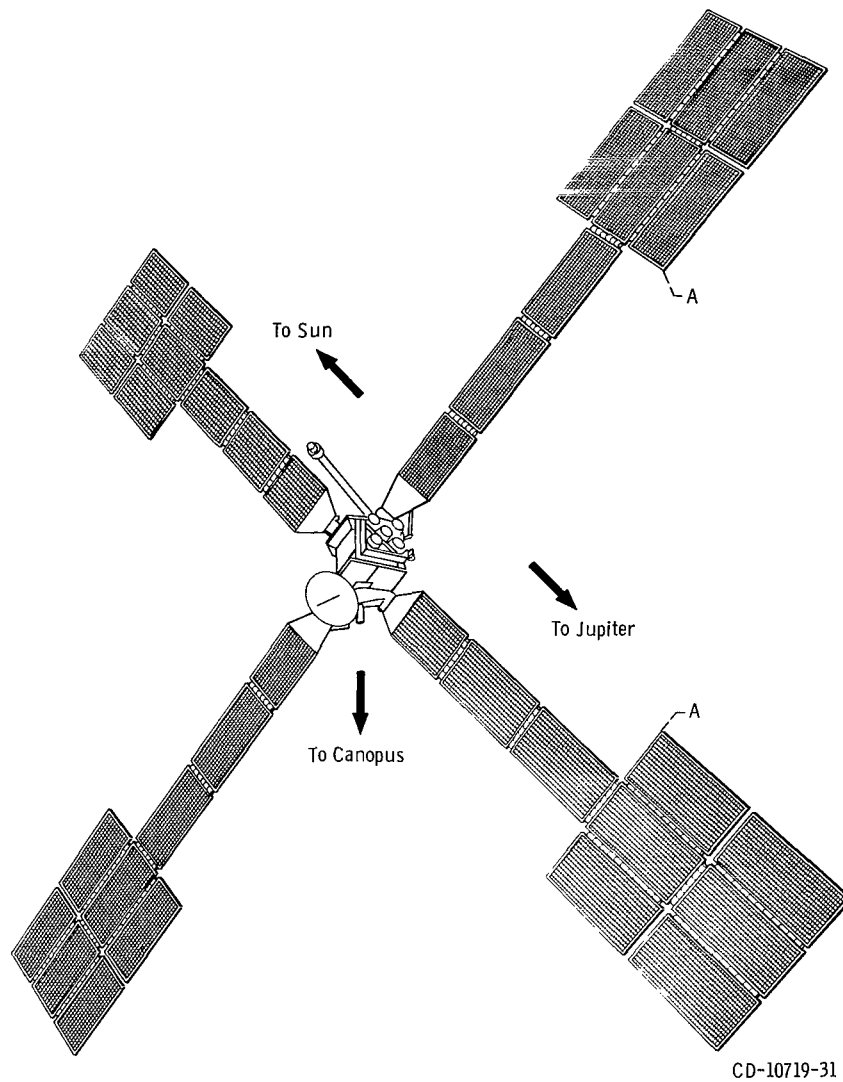
CD-10719-31

Figure 11. – Jupiter solar electric spacecraft (ref. 12).

of the ion beam envelope. The tolerable ion impingement on solar cells is not known. Little is known of the interaction of mercury ions with solar cells.

CONCLUDING REMARKS

A collimating slit system was used to measure the ion beam envelope and to deter-mine the thrust vector of an electron-bombardment ion thruster of the SERT II type.

The ion beam envelope was measured for five cases which included variation of grid

alinement, grid spacing, accelerator grid voltage, and ion beam current. It was found that the ion beam envelope was sensitive to the thruster operating conditions. For the standard thruster configuration, the maximum dispersion angle at which ion current was measured was 39°. The variations in thruster configuration led to variation in the maximum dispersion angle between 27° and 45°.

The thrust direction was measured for the standard and misalined grid thruster configurations. The measured shift in thrust direction with grid misalinement was about 7.6^O and was in good agreement with results from a previous theoretical study (ref. 2) and a previous experimental investigation (ref. 4).

To illustrate the importance of definition of the ion beam envelope, the results of this investigation were applied to a spacecraft design for a proposed Jupiter flyby mission. It was found that ion impingement would occur on part of the solar cells for more than 130 days of the mission with this spacecraft design.

Lewis Research Center,
    National Aeronautics and Space Administration,
        Cleveland, Ohio, March 18, 1970,
            120-26.

APPENDIX A

SYMBOLS

A surface of revolution defined by locus of rear slit, m^2

C capacitance, F

C_1 conversion constant, defined in eq. (B12)

D distance between collimating slits, m

$\bar{I}$ general ion vector

$\bar{I}_{rz}$ component of general ion vector in $\bar{R}, \bar{Z}$ plane

I_T total thruster ion current, A

$I(R, \theta)$ measured ion current, A

$I(R)_p$ ion current through plane $\bar{P}$, A

J_B ion beam current, A

J_I discharge chamber current, A

$j(R)_p$ current density, defined in eq. (B2)

$j_I(R, \theta)$ current density, defined in eq. (B1)

L slit length, m

l grid-to-grid spacing, mm

$\bar{P}$ plane of measurement, defined in fig. 1

R vertical slit system position, cm

$\mathscr{R}$ resistance, ohm

$\bar{R}$ coordinate direction, defined in fig. 1 and sketch (a)

$\bar{R}'$ coordinate direction, defined in fig. 1

r vertical distance in plane of accelerator grid, defined in sketch (a), m

T thrust

t time, sec

$V(R, t)$ input to analog computer from collimating slit, V

V_A accelerator grid voltage, V

$V_c(R)$ integrated output of analog computer, V

V_I net accelerating voltage, V

ΔV_I discharge chamber voltage, V

W slit width, m

$\bar{Z}$ coordinate direction, defined in fig. 1 and sketch (a)

α defined in fig. 12

β defined in sketch (a)

θ dispersion angle, defined in sketch (a) and fig. 12

ξ defined in fig. 12

Φ angle of thrust vector in $\bar{R}, \bar{Z}$ plane, defined in eq. (B18)

ψ defined in sketch (a)

Subscripts:

a   axial

L   local (at particular vertical R location)

p   plane $\overline{P}$

r   radial

APPENDIX B

ANALYSIS OF COLLIMATING SLIT SYSTEM

This appendix describes the experiment coordinate system, the procedure used to obtain local ion current densities as a function of dispersion angle, and the analyses used to obtain the total ion current and thrust vector direction from the slit system data.

Experiment Coordinate System

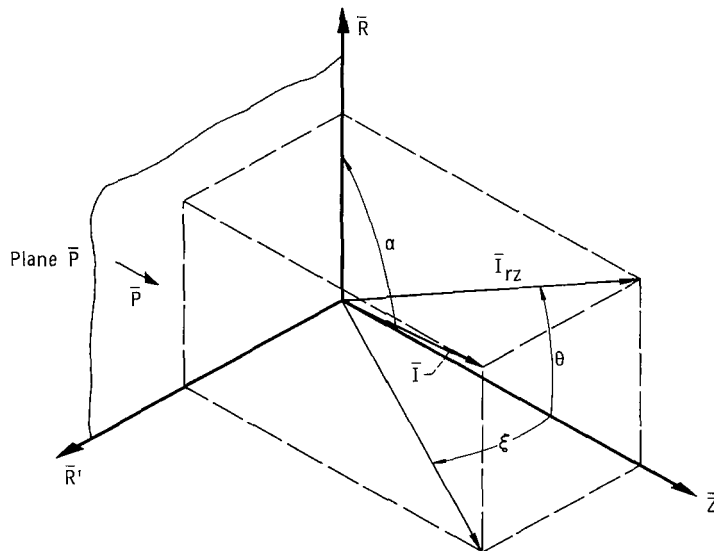The coordinate system shown in figures 1 and 12 was found convenient to describe

Figure 12. – Coordinate system. (Thruster axis is along $\bar{Z}$ axis (see fig. 1).)

the experiment. The $\bar{Z}$ axis was along the longitudinal axis of the thruster. The $\bar{R}$ axis was perpendicular to the $\bar{Z}$ axis and located in the $\bar{P}$ plane which was 29.4 centimeters downstream of the accelerator grid of the thruster. To a good approximation, the $\bar{R}$ axis was parallel to the locus of vertical points at which the ion beam was sampled with the collimating slit system. The $\bar{R}'$ axis was perpendicular to the $\bar{Z}$ and $\bar{R}$ axes. The $\bar{R}'$ axis was parallel to the long axis of both the front and rear collimating slits and also parallel to the axis of the support shaft (axis of rotation of the collimating slit system).

In general, an ion can have a velocity vector with a component in each of the three coordinate directions. Figure 12 shows a general ion vector designated as $\overline{I}$. The components of the ion velocity vector in the $\overline{R}$, $\overline{Z}$, and $\overline{R}'$ directions are $|I| \cos \alpha$, $|\overline{I}| (\sin \alpha)(\cos \xi)$, and $|\overline{I}| (\sin \alpha)(\sin \xi)$, respectively. The $\overline{I}$ vector projected into the $\overline{R}, \overline{Z}$ plane is shown as $\overline{I}_{rz}$. The angle between $\overline{I}_{rz}$ and the $\overline{Z}$ axis is shown as θ.

The product $|\overline{I}_{rz}| \cos \theta$ is the component of the ion current in the $\overline{Z}$ (or axial) direction and the product $|\overline{I}_{rz}| \sin \theta$ the component of the ion current in the $\overline{R}$ direction. The latter component is referred to as the radial component in this report.

The collimating slit system was used herein to evaluate the ion current distribution as a function of angle (the dispersion angle) at various vertical positions. Because of the narrow slit width, at a fixed collimating slit position, ions were collected that had values of θ very near some mean value. The mean value of θ about which ions were collected was varied by rotation of the slit system.

Unless otherwise specified, it was assumed that ions in the beam had no component in the $\overline{R}'$ direction. This is equivalent to an assumption that the ion trajectories were parallel to the $\overline{R}, \overline{Z}$ plane. With this assumption local values of axial ($\overline{Z}$ direction) and radial ($\overline{R}$ direction) components of thrust could be calculated from measurements made with the collimating slit system.

The assumption that the $\overline{R}'$ component of velocity was zero did result in errors in calculated local values of the thrust vector and ion current density. Discussion of these errors is presented in appendix C where it is shown that the error in the estimate of thrust vector was very small. Measured values of local ion current density were low due to the presence of $\overline{R}'$ components.

Local Ion Current as a Function of Dispersion Angle

One purpose of this experiment was to determine the angular properties of the ion beam at various vertical positions which were approximately located along a diameter of the thruster. The slit system was located at the various vertical positions by pivoting the slit system support shaft about a pivot located in the bell jar wall (fig. 1). With the locating apparatus used, the front slit was always in the $\overline{P}$ plane. The arrangement is discussed more completely in the APPARATUS section.

As stated previously, ion current was measured if it passed through both the front and rear slits and arrived at the collector. At a fixed slit position, ions would pass through both slits only if they were within about 2^O of some mean dispersion angle. Measurement of ion current as the slit system was rotated then allowed an evaluation of the local ion current as a function of dispersion angle.

The ion current measured at a fixed slit position $I(R, \theta)$ was used to define an average ion current density in the direction θ as

$$j_I(R, \theta) = \frac{I(R, \theta)}{LW} \tag{B1}$$

where

$j_I(R, \theta)$ average ion current density in directions, A/m^2

$I(R, \theta)$ ion current measured, A

L   length of front slit, m

W   width of front slit, m

The various x-y plotter traces presented in figures 5 and 10 show the ion current density as a function of dispersion angle. The ion current $I(R, \theta)$ was obtained from the ordinate of the x-y plotter trace.

Total Thruster Ion Current

The total ion current from the thruster was determined by integration of the local ion current densities obtained with the collimating slit system. Comparison of the total ion current thus calculated with the total ion current measured with an ammeter provided an indirect check on the accuracy of the collimating slit system.

In order to determine the total ion current from the thruster with the slit system, it was necessary to calculate the total ion current through the plane $\overline{P}$. Figure 13 is a simplified view of the slit system useful in discussion of this calculation. For clarity, many features, such as the separation block have been omitted. To calculate the total current through the plane $\overline{P}$, it is necessary to determine the local ion current density in plane $\overline{P}$. The local current density is given by the relation

$$j(R, \theta)_p = \frac{I(R, \theta)\cos \theta}{LW} \tag{B2}$$

where the $\cos \theta$ is an area correction factor to give the equivalent current through an area LW in plane $\overline{P}$.

As seen from figure 13, values of ion current $I(R, \theta)$ are measured on a cylinder of revolution defined by the locus of the rear slit during rotation of the slit system. The cylinder of revolution is at a distance D from the front slit and is of length L. Equation (B2) can be taken to represent the ion current density on the surface of revolution due to ions which passed through an opening LW in plane $\overline{P}$.
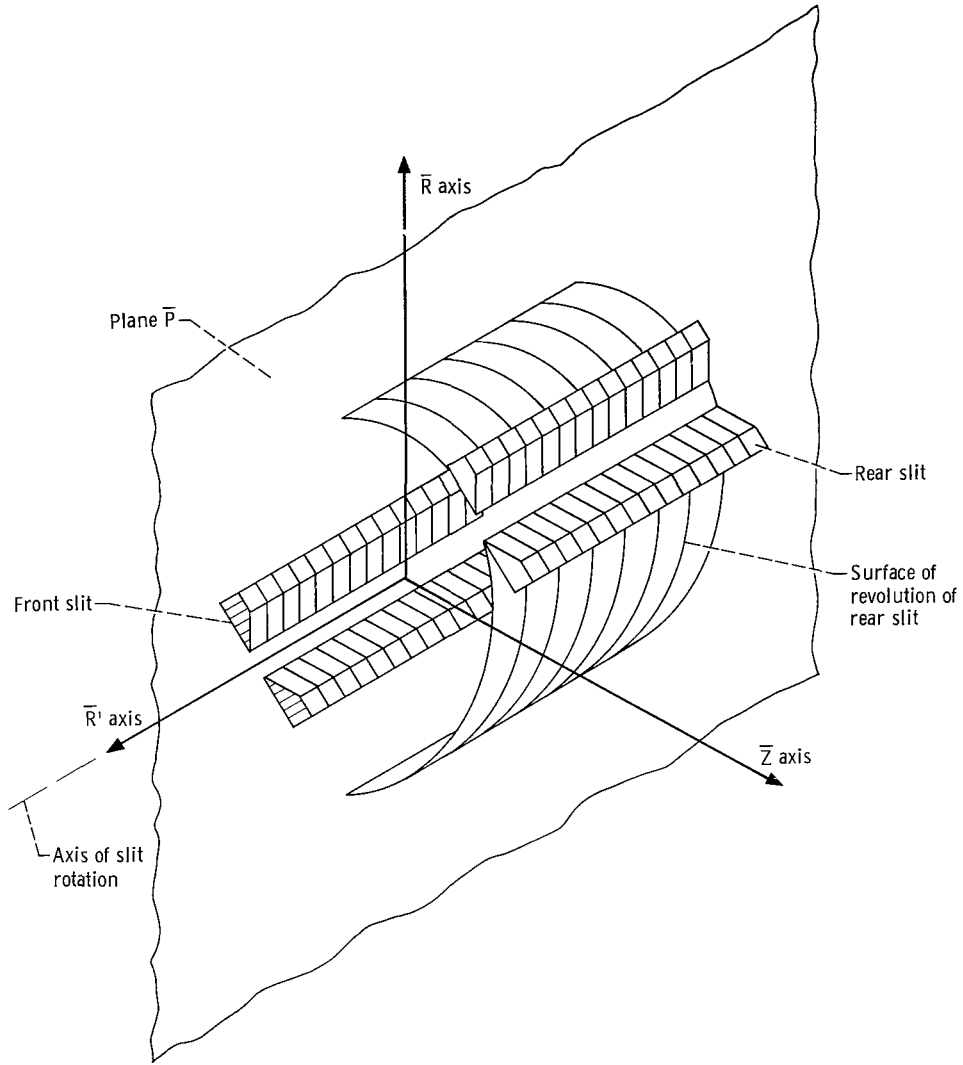
Figure 13. - Cutaway of slit system.

The total current through plane $\overline{P}$ at the vertical data point location is just the integral of the current density of equation (B2), $j(R, \theta)_p$, over the cylinder of revolution, that is,

$$I(R)_p = \int_A j(R, \theta)_p \, dA = \int_A \frac{I(R, \theta)\cos \theta \, dA}{LW} \tag{B3}$$

where

$I(R)_p$ total current through plane $\overline{P}$ at vertical data point location, A

dA incremental area of the surface of revolution, m^2

Since

$$dA = LD\, d\theta$$

$$I(R)_p = \frac{D}{W} \int_{\theta_1}^{\theta_2} I(R, \theta)\cos\theta\, d\theta \qquad (B4)$$

where θ_1 and θ_2 are limits of the dispersion angle over which ion current is collected.

The local current density is just the current of equation (B4) divided by the area of the front slit or

$$j(R)_p = \frac{D}{LW^2} \int_{\theta_1}^{\theta_2} I(R, \theta)\cos\theta\, d\theta \qquad (B5)$$

The current density of equation (B5) is identical to that which would be obtained with a planar probe whose dimensions are equal to that of the front slit and whose surface lies in the plane $\overline{P}$.

As the support shaft rotated, the angle θ varied in a known manner with time. The current in the integrand of equation (B5) was then a function of time and for the scale factors used in this experiment was

$$I(R, \theta) = I(R, t) = 10^{-5}\, V(R, t) \qquad (B6)$$

where $V(R, t)$ was a measured value of the experiment.

The speed of rotation of the slit system was constant to within about 0.2 percent and for this experiment was

$$\frac{\Delta\theta}{\Delta t} = 7.24 \times 10^{-2} \quad \frac{\text{rad}}{\text{sec}} \qquad (B7)$$

Substitution of the slit system geometrical dimensions and equations (B6) and (B7) into equation (B5) yields

$$j(R)_p = 1.6 \int_{t_1}^{t_2} \cos(\theta, t)V(t)\, dt \qquad (B8)$$

The output of the analog computer was just

$$V_c(R) = \frac{1}{\mathscr{R}C} \int_{t_1}^{t_2} \cos(t)V(t)\, dt \qquad (B9)$$

29

The product of $\mathscr{R}$ and C was unity for this experiment so that the local ion current density from the thruster was

$$j(R)_p = 1.6\, V_c(R)\ \frac{A}{m^2} \tag{B10}$$

The current density of equation (B10) was plotted in figure 7 as a function of vertical distance at which local measurements were taken. As seen in figure 7, a small asymmetry existed about the longitudinal axis of the thruster (R = 0). In order to account for the small asymmetry, the curves of figure 7 were divided into 1-centimeter increments on each side of R = 0. An average value of ion current density in a particular 1-centimeter increment was taken to be the value at the midpoint of the increment. The average current density over an annular ring in plane $\overline{P}$ was taken to be the average value of the midpoint values of the corresponding 1-centimeter increments on each side of R = 0. The total ion current from the thruster was then

$$I_T = \pi \sum_{x=0}^{n} \overline{j}(R)_p\ (R_{x+1}^2 - R_x^2) \tag{B11}$$

The total ion current from the thruster was computed for the standard case I and case III (low accelerator voltage). The values of the total current thus evaluated for these two cases were 219 and 222 milliamperes, respectively. The output current was measured with an ammeter as 242 and 240 milliamperes, respectively, for cases I and II. It is seen that the currents evaluated for the two cases were about 9 percent lower than the ammeter values. Possible sources of error are discussed in appendix C.

Thrust Vector

The local values of the components of thrust were obtained and utilized to determine the total thrust vector. The local components of thrust were obtained from measurements made in plane $\overline{P}$ in a band, of length L, which was nearly parallel to a diameter of the thruster. The local radial and axial components of thrust per unit vertical distance R due to ion current in the direction θ are, respectively

$$T_{rL}(R, \theta) = C_1\, \frac{I(R, \theta)\cos\theta\,\sin\theta}{W} \tag{B12}$$

$$T_{aL}(R, \theta) = C_1\, \frac{I(R, \theta)\cos^2\theta}{W} \tag{B13}$$

where C_1 is a conversion constant that relates the ion current to thrust and includes the effect of the net accelerating voltage and ion species.

It was assumed in equations (B12) and (B13) that the slit width W represented the vertical distance dR over which data were sampled at each local location.

By arguments similar to those of the preceding section, the local radial and axial components of thrust per unit vertical distance are

$$T_{rL}(R) = \frac{C_1 D}{W^2} \int_{\theta_1}^{\theta_2} I(R, \theta)\cos\theta \sin\theta \, d\theta \tag{B14}$$

$$T_{aL}(R) = \frac{C_1 D}{W^2} \int_{\theta_1}^{\theta_2} I(R, \theta)\cos^2\theta \, d\theta \tag{B15}$$

The total radial and axial components of thrust, in the band of measurement, L wide in plane $\overline{P}$, are just the integrals over the vertical distance R of equations (B14) and (B15)

$$T_r = C_1 \frac{D}{W^2} \int_R dR \int_{\theta_1}^{\theta_2} I(R, \theta)\cos\theta \sin\theta \, d\theta \tag{B16}$$

$$T_a = C_1 \frac{D}{W^2} \int_R dR \int_{\theta_1}^{\theta_2} I(R, \theta)\cos^2\theta \, d\theta \tag{B17}$$

The angle of the thrust vector with respect to the longitudinal axis of the thruster over the region of measurement is obtained from equations (B16) and (B17)

$$\Phi = \arctan \frac{T_r}{T_a} \tag{B18}$$

For the data presented in this report, equations (B16) and (B17) were modified since the integrals of these equations were not produced with available experimental apparatus. At each radial location the range of dispersion angles over which ion current was collected was available from the x-y plotter traces. For example, the range of dispersion angles varied from $\pm 15^{\circ}$ at $R = 0$ to about 25° to 37° at $R = +21.1$ centimeters (fig. 5(d)) for the standard case. At each radial location, the quantity $\cos\theta$ in the integrands of equations (B16) and (B17) was replaced with an average value of $\cos\theta$ over the range of dispersion angles over which ions were collected. The average value of $\cos\theta$ was taken to be that corresponding to the midpoint of the range of dispersion angle.

A cursory analysis indicated that use of an average cosine introduced negligible error into equations (B16) and (B17).

The value of local radial and axial component of thrust shown in figure 8 were

$$T_{rL}(R) = \overline{\cos\theta}\ (R)\ \frac{C_1 D}{W^2}\ \int_{\theta_1}^{\theta_2} I(R,\theta)\sin\theta\ d\theta \tag{B19}$$

$$T_{aL}(R) = \overline{\cos\theta}\ (R)\ \frac{C_1 D}{W^2}\ \int_{\theta_1}^{\theta_2} I(R,\theta)\cos\theta\ d\theta \tag{B20}$$

The local values of radial and axial component of thrust given in equations (B19) and (B20) with the constants C_1, D, and W eliminated, were plotted as a function of R in figure 8. The integrals of these curves were then taken with a planimeter. The ratio of the integrals thus obtained then yielded the direction of the total thrust vector over the region of measurement (eq. (B18)).

APPENDIX C

DISCUSSION OF ERRORS

The errors to be discussed in this section are those peculiar to the particular collimating slit system used. For the configuration utilized errors might arise due to secondary electron emission, space charge spreading of the ion beam in the slit system, and the presence of asymmetric ion trajectory. These possible sources of error will be discussed separately.

Secondary Electron Emission

Secondary electrons could be produced when the ion beam strikes the collector or suppressor grid. It was found that the collector current would decrease by a few percent when the suppressor grid bias (fig. 4) with respect to the collector was varied from 0 to about -5 volts. This reduction was probably due to suppression of secondary electrons from the collector. In order to prevent the emission of secondary electrons from the collector, the suppressor grid was biased -20 volts with respect to the collector for all the data presented in the report. Secondary electrons could be emitted from the suppressor grid. However, since the suppressor grid represented only about 12 percent of the total collector area, the effect of such secondaries was considered negligible. This assumption is strengthened by the fact that the values of integrated ion beam current were about 10 percent lower than values recorded directly with an ammeter. The presence of secondary electrons would have led to integrated values of ion current higher than the metered values.

Space Charge Spreading

Under certain conditions, significant ion beam spreading might occur in the collimating slit system. This spreading would tend to lower the values of collected current and hence would lead to lower calculated values of total ion current. The problem of beam spreading has been examined in reference 18, and reference 19 gives a simplified approximation of the results of reference 18. Due to the complexity of the present experiment, the problem has not been evaluated analytically and the magnitude of the problem, if any, is not known. From examination of available literature the effect is thought to be small.

Effect of Components in the $\overline{R}'$ Direction

It was pointed out previously that the collimation slit system could resolve ion current in only two directions. At a fixed slit system position, ion current passed through both slits only if the values of θ associated with the trajectories were contained within $2^O2'$ of the mean dispersion angle. In general, ion trajectories probably had a component in the $\overline{R}'$ direction (and an associated value of ξ (fig. 12)).

The presence of components of ion current in the $\overline{R}'$ direction could influence the evaluation of the local values of both the ion current density and the thrust vector. Discussion of this point is aided by reference to figure 14.
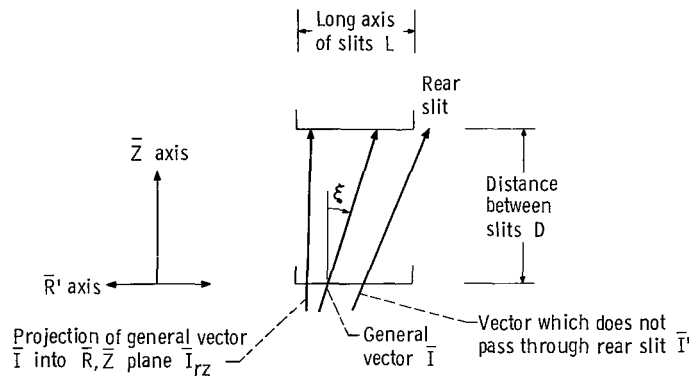

Figure 14. - View of slits in $\overline{R}', \overline{Z}$ plane. (R axis perpendicular to $\overline{R}'$ and $\overline{Z}$ axes.)

Figure 14 is a section view of the slit system taken parallel to the $\overline{R}', \overline{Z}$ plane. The collimating slit is shown located on the axis of the thruster (R = 0) and oriented at a dispersion angle of 0° ($\theta = 0$). For reference two velocity vectors are shown. One is a general velocity vector $\overline{I}$ which represents an ion that enters the front slit (at angle ξ), passes through the rear slit, and is collected. The component of I parallel to the $\overline{R}, \overline{Z}$ plane is $\overline{I}_{rz}$. A second vector I' is shown which, due to the value of ξ associated with it and the location along the $\overline{R}'$ axis at which it enters the front slit, passed through the front slit but not through the rear slit.

Because some ions which passed through the front slit may not have been collected, the collimating slit system measurement could yield values that underestimate the local ion current. Evaluation of this possible error would require exact knowledge of the angular distribution of the ion current in the ξ direction. It was seen that the total ion current calculated from the collimating slit results was about 9 percent lower than the ion current indicated by ammeters. In the opinion of the author it is likely that this result was due in part to the effect just described. Although no data is available, an esti-

mate of the worst case error in the thrust vector was made by assuming that all the ion current entered the slit system from the furthest extremity of the source area (r = 6.95). The resulting angle would be about 15.7^O for this geometry. The error in the axial component of thrust would then be

$$\text{Error} = \frac{I(1 - \cos \xi)}{I} = 0.037 \tag{C1}$$

Clearly, the actual error must be much less for the real case and for this reason was neglected in this report.

REFERENCES

1. Kerrisk, D. J.; and Kaufman, H. R.: Electric Propulsion Systems for Primary Spacecraft Propulsion. Paper 67-424, AIAA, July 1967.

2. Seliger, R. L.; Nudd, G. R.; Brewer, G. R.; and Amboss, K.: Analysis of the Expected Thrust Misalignment of Kaufman Thrusters. Paper 69-303, AIAA, Mar. 1969.

3. Lathem, Walter C.: Effects of Electrode Misalinements in Kaufman Thrusters. J. Spacecraft Rockets, vol. 5, no. 6, June 1968, pp. 735-737.

4. Sohl, Gordon; and Fosnight, Verryl V.: Thrust Vectoring of Ion Engines. J. Spacecraft Rockets, vol. 6, no. 2, Feb. 1969, pp. 143-147.

5. Byers, David C.; and Staggs, John F.: SERT II Flight-Type Thruster System Performance. Paper 69-235, AIAA, Mar. 1969.

6. Richley, Edward A.; and Kerslake, William R.: Bombardment Thruster Investigations at the Lewis Research Center. J. Spacecraft Rockets, vol. 6, no. 3, Mar. 1969, pp. 289-295.

7. Reynolds, Thaine W.; and Richley, Edward A.: Propellant Condensation on Surfaces Near an Electric Rocket Exhaust. J. Spacecraft Rockets, vol. 6, no. 10, Oct. 1969, pp. 1155-1161.

8. Hall, David F.; Newnam, Brian E.; and Womack, James R.: Electrostatic Rocket Exhaust Effects on Solar-Electric Spacecraft Subsystems. Paper 69-271, AIAA, Mar. 1969.

9. Byers, David C.; Kerslake, William R.; and Grobman, Jack: Experimental Investigation of Heavy-Molecule Propellants in an Electron-Bombardment Thrustor. NASA TN D-2401, 1964.

10. Pugmire, T. K.: Design, Development, Fabrication, Test, and Delivery of Electrothermal Engine Systems. Rep. AVSSD-0062-68-RR, Avco Corp. (NASA CR-72362), Nov. 1967.

11. Stevenson, D. P.; and Schissler, D. O.: Mass Spectrometry and Radiation Chemistry. The Chemical and Biological Action of Radiations. Vol. 5. M. Haïssinsky, ed., Academic Press, 1961, pp. 167-271.

12. Barber, T.; et al.: 1975 Jupiter Flyby Mission Using a Solar Electric Spacecraft. Rep. ASD 760-18, Jet Propulsion Lab., California Inst. Tech., Mar. 1, 1968.

13. Bechtel, Robert T.: Discharge Chamber Optimization of the SERT II Thruster. J. Spacecraft Rockets, vol. 5, no. 7, July 1968, pp. 795-800.

14. Staggs, John F.; Gula, William P.; and Kerslake, William R.: Distribution of Neutral Atoms and Charge-Exchange Ions Downstream of an Ion Thruster. J. Spacecraft Rockets, vol. 5, no. 2, Feb. 1968, pp. 159-164.

15. Reynolds, Thaine W.; and Richley, Edward A.: Thermionic Emission from Cesium-Coated Electrostatic Ion-Thrustor Electrodes. NASA TN D-1879, 1963.

16. Pawlik, Eugene V.; Margosian, Paul M.; and Staggs, John F.: A Technique for Obtaining Plasma-Sheath Configurations and Ion-Optics for an Electron-Bombardment Ion Thrustor. NASA TN D-2804, 1965.

17. Jack, John R.; and Spisz, Ernie W.: Thermal Radiative and Electrical Properties of a Cadmium Sulfide Solar Cell at Low Solar Intensities and Temperatures. NASA TN D-4818, 1968.

18. Spangenberg, Karl R.: Vacuum Tubes. McGraw-Hill Book Co., Inc., 1948, ch. 15.

19. Fleischmann, H. H.; Ashby, D. E. T. F.; and Larson, A. V.: Errors in the Use of Mass Analyzers in Plasma Physics. Nucl. Fusion, vol. 5, 1965, pp. 349-351.

"The aeronautical and space activities of the United States shall be conducted so as to contribute . . . to the expansion of human knowledge of phenomena in the atmosphere and space. The Administration shall provide for the widest practicable and appropriate dissemination of information concerning its activities and the results thereof."

— NATIONAL AERONAUTICS AND SPACE ACT OF 1958

NASA SCIENTIFIC AND TECHNICAL PUBLICATIONS

TECHNICAL REPORTS: Scientific and technical information considered important, complete, and a lasting contribution to existing knowledge.

TECHNICAL NOTES: Information less broad in scope but nevertheless of importance as a contribution to existing knowledge.

TECHNICAL MEMORANDUMS: Information receiving limited distribution because of preliminary data, security classification, or other reasons.

CONTRACTOR REPORTS: Scientific and technical information generated under a NASA contract or grant and considered an important contribution to existing knowledge.

TECHNICAL TRANSLATIONS: Information published in a foreign language considered to merit NASA distribution in English.

SPECIAL PUBLICATIONS: Information derived from or of value to NASA activities. Publications include conference proceedings, monographs, data compilations, handbooks, sourcebooks, and special bibliographies.

TECHNOLOGY UTILIZATION PUBLICATIONS: Information on technology used by NASA that may be of particular interest in commercial and other non-aerospace applications. Publications include Tech Briefs, Technology Utilization Reports and Notes, and Technology Surveys.

Details on the availability of these publications may be obtained from:

SCIENTIFIC AND TECHNICAL INFORMATION DIVISION

NATIONAL AERONAUTICS AND SPACE ADMINISTRATION
Washington, D.C. 20546